BMR Journal of Australian Geology & Geophysics, 13, 275–279


# Depth phases from local earthquakes

Günter Bock[1]

Synthetic seismogram modelling and observations suggest that depth phases from local crustal earthquakes are of the type *sX*, where *X* stands for $P_g$, $P_n$, and the reflections from the crust-mantle boundary, mainly $P_MP$ and $S_MS$. Depth phases of the type *pX* generally have much smaller amplitudes and are unlikely to stand out in seismograms. The differential times *sX*–X provide a very good control of focal depth. Examples of earthquakes that occurred in May and June 1991 in an area northwest of Kempsey (New South Wales) and in September 1991 near St George (Queensland) indicate that their foci were in the uppermost crust, at depths of between 2 and 3 km.

## Introduction

Focal depths of Australian earthquakes are usually poorly constrained. Most, if not all earthquakes have their foci in the upper crust, at depths not deeper than about 20 km. Good depth control is normally provided by data of stations that are located close to the epicentre. This favourable condition is rarely met in Australia.

Accurate depth estimates have been obtained for large earthquakes and some of their foreshock and aftershock sequences in central and western Australia using waveform analysis of local and teleseismic seismograms and data of temporary seismic networks (Langston, 1987; Fredrich & others, 1988; Bowman & others, 1990; Choy & Bowman, 1990). Langston (1987) used the depth phase $sP_g$ and the ratio $Rg/S_g$ observed at distances of less than 100 km to constrain focal depths of events in the 1968 Meckering earthquake sequence. He showed that most foreshocks and aftershocks occurred within 2 km of the surface.

Most weak earthquakes in Australia usually do not attract attention far beyond the realm of routine interpretation. In the absence of reliable constraints, focal depths are often fixed to a value chosen by the interpreter. An improved knowledge of the depth distribution of earthquakes, however, is of considerable importance in seismotectonic studies of the Australian continent.

It is the purpose of this paper to discuss depth-sensitive phases from crustal earthquakes at distances to several hundred kilometres, which may provide a much improved depth control over what is possible with first arrival time data only. The successful identification of such phases is considerably aided, and in the experience of the author only possible in many cases, if digital seismograms are available. In this paper, synthetic seismograms are presented that tell us which depth-sensitive phases we may expect to see on seismograms. Examples from the Armidale (New South Wales) seismograph station, where a PC-based data logger has been successfully tested for more than a year, are then discussed.

## Synthetic seismograms

Synthetic seismograms have been calculated for a shear dislocation point source using the reflectivity method of Kind (1978, 1979a). The crustal gradient model used is shown in Table 1. A crustal thickness of 33 km is assumed which is based on seismic refraction studies in the New England Orogen described by Finlayson & Collins (in press). Synthetic seismogram sections are shown (Figs 1, 2) for two different distance ranges.

Seismograms from a 3 km deep source (Fig. 1) are shown for the distance range from 70 to 140 km. A dip slip shear dislocation was assumed along a plane dipping at 45° towards the receivers. The crustal phase $P_g$ is the first arrival followed about 0.6 s later by a second phase which, based on travel time, is the surface reflection $sP_g$. This is a phase which has left the focus upwards as an *S* wave, been converted at the surface to a *P* wave, and then has travelled the remaining path to the receivers as *P* entirely confined to the upper crust.

Following the $P_g$ wavegroup another set of phases arrives between 2 s and 5 s reduced time. The first phase has the travel time of the Moho reflection $P_MP$. Its amplitude is

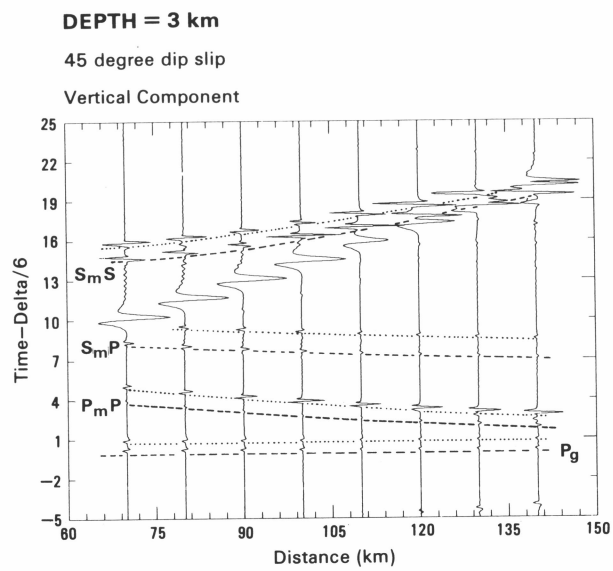


**Figure 1. Synthetic seismograms for a 45° dip slip point source at 3 km depth.**
The arrival times of various crustal phases have been marked by the dashed lines; the associated depth phases of type *sX*, where *X* stands for $P_g$, $P_MP$, $S_MP$ or $S_MS$ are marked by dotted lines.

**Table 1. Crustal gradient model.**

| *Depth (km)* | *P-wave velocity (km/s)* | *S-wave velocity (km/s)* | *Density (g/cc)* | *QP* | *QS* |
|---|---|---|---|---|---|
| 0 | 6.00 | 3.53 | 2.53 | 1000 | 444 |
| 12.5 | 6.00 | 3.53 | 2.53 | 1000 | 444 |
| 22 | 6.15 | 3.61 | 2.58 | 1000 | 444 |
| 33 | 6.45 | 3.79 | 2.70 | 1000 | 444 |
| 33 | 7.70 | 4.46 | 3.17 | 1000 | 444 |
| 45 | 7.80 | 4.50 | 3.21 | 1000 | 444 |
| 60 | 8.08 | 4.66 | 3.31 | 1000 | 444 |
| 92 | 8.12 | 4.69 | 3.33 | 1000 | 444 |

[1] GeoForschungsZentrum, Telegrafenberg A6, O-1561 Potsdam, Germany; formerly Department of Geology and Geophysics, University of New England, Armidale NSW 2351

small because $P$ wave radiation is weak in the takeoff direction of $P_MP$ for the 45° dip slip source used in the calculations. About 1 s after $P_MP$ a second, large-amplitude phase arrives. Its arrival time suggests that it is the surface reflection $sP_MP$ which leaves the focus upwards as an $S$ wave, is converted at the surface to $P$, and then follows along the $P_MP$ path to the receivers. The amplitude of $P_MP$ is sensitive to the radiation pattern. Assuming a vertical strike slip dislocation, for example, $P_MP$ and $sP_MP$ reach similar amplitudes.

Another reflection from the crust-mantle boundary and associated depth phase shows up in Figure 1 between 7 s and 10 s reduced time. The earlier phase fits the travel time of $S_MP$ while the phase arriving about 1.5 s after $S_MP$ is the surface reflection $sS_MP$.

The Moho reflection $S_MS$ and associated depth phase $sS_MS$ shows up between 15 s and 20 s reduced time; it interferes at larger distances with the surface wave arrival $R_g$.

The synthetic seismogram section in Figure 2 covers the distance range from 250 to 450 km. A vertical strike slip dislocation source at 6 km depth was assumed, with the receivers located at 45° azimuth to the strike of the fault plane. The first arrivals are upper mantle phases ($P_n$) that are followed about 2.5 s later by a second phase which fits the travel time for the surface reflection $sP_n$. The phase $sP_n$ has been discussed by other authors (Kind, 1979b; Zonno & Kind, 1984; Barbano & others, 1985), and has been used by Bock (in press) to constrain the focal depth of the 1990 Woods Reef earthquake. If $sP_n$ can be correctly identified it provides a stringent constraint on focal depth. As noted by Bock (in press) the amplitude ratio $P_n/sP_n$ depends strongly on the source mechanism. For a 45° dip slip source, for example, the $P_n$ amplitude becomes quite small compared to $sP_n$. In this case $P_n$ may go unnoticed, especially for weaker earthquakes, and $sP_n$ may be picked as first arrival and erroneously interpreted as $P_n$.

Other depth phases in Figure 2 are associated with $P_g$, $S_n$ and multiple reflections from the crust-mantle boundary.

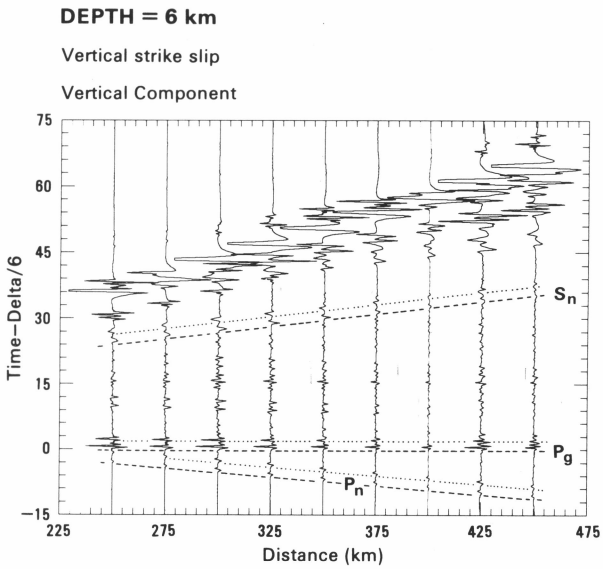


**Figure 2. Synthetic seismograms for a strike slip point source along a vertical plane at 6 km depth.**
Dotted lines indicate depth phases of type $sX$ associated with $P_n$, $P_g$ and $S_n$.

Some of these phases are identified in Figure 2. The occurrence of multiple reflections from the Moho depends on many factors such as crustal thickness, crustal velocities and sharpness of the crust-mantle transition. Their actual arrival times and amplitudes are clearly subject to regional variations. The differential times between these phases and associated depth phases however are much less dependent on regional variations in crustal structure; they are therefore well suited as depth constraint if they can be reliably identified.

Note that in all the cases discussed in this section the depth phases are of the type $sX$, where $X$ stands for $P_g$, $P_n$, or reflections from the Moho. Depth phases of the type $pX$ are unlikely to stand out with significant amplitude because the $P$–$P$ reflection coefficient for the free surface is small over a range of angles of incidence (Aki & Richards, 1980, 142). The $S$–$P$ reflection coefficient of the free surface, on the other hand, reaches large values particularly if the angle of incidence is near critical.

## Examples

### Armidale seismograph

In this section, recordings of several earthquakes that occurred in eastern Australia in 1991 are discussed with regard to the presence of depth phases. The observations are from the vertical-component, short-period Armidale seismograph which is part of the National Seismograph Network operated by the Australian Seismological Centre (ASC). The seismometer was located until September 1991 in the Cooney (COO) tunnel at 30.568°S, 151.884°E, approximately 25 km east of Armidale. In September 1991 it was shifted to a new location at Newholme, about 7 km north of Armidale (ARMA, 30.420°S, 151.628°E). A telephone line has been used to transmit the seismometer signal to the recording site in the Department of Geology and Geophysics of the University of New England where seismograms are routinely recorded as Helicorder chart records.

Since April 1991, recordings of most earthquakes have been obtained also as digital records. This was achieved by digitising the output of the demodulator at the recording site using a 12 bit analogue-digital converter (ADC) connected to an AT compatible microcomputer. A data acquisition program written in Quickbasic by Boggs (1991) is based on the comparison of short term average (STA) and long term average (LTA) values of the seismic signal as described by McEvilly & Majer (1982). If the STA exceeds the LTA by a prescribed value, an event is indicated and the data are stored with a sample frequency of 50 Hz to hard disk. The dynamic range of the digital record is of course limited by the analogue recording system. Furthermore, data are recorded over a narrow frequency band because of the filter settings for the analogue system. Therefore, the quality of the Armidale digital records is poor by comparison to those obtained from state of the art broadband seismographs. Nevertheless, the availability of a digitised copy of the analogue seismogram leads to a dramatic improvement in data quality, and much more information can be extracted from the digital records than is possible with chart recordings as demonstrated by the following examples.

### The 1991 Kempsey earthquakes

The first example is from a series of three earthquakes that occurred in 1991 on May 21, 0324 Universal Coordinated

Time (UTC), May 23, 2134 UTC, and June 11, 0740 UTC. All events were recorded by the Cooney station (COO). The May 21 event was the strongest ($M_L$ = 2.3) in the series. Its epicentre was located at 31.0°S and 152.6°E, some 25 km northwest of Kempsey (New South Wales). This location, however, is very poorly constrained.

The digital COO seismograms of the events that are shown in Figure 3 are very similar, which suggests that the two later events were located close to the first one. Several distinct phases are visible. The largest-amplitude phase is the surface wave arrival marked *Rg*. Its signal contains relatively low frequencies, and there is an indication that higher-frequency signals are superimposed on the *Rg*

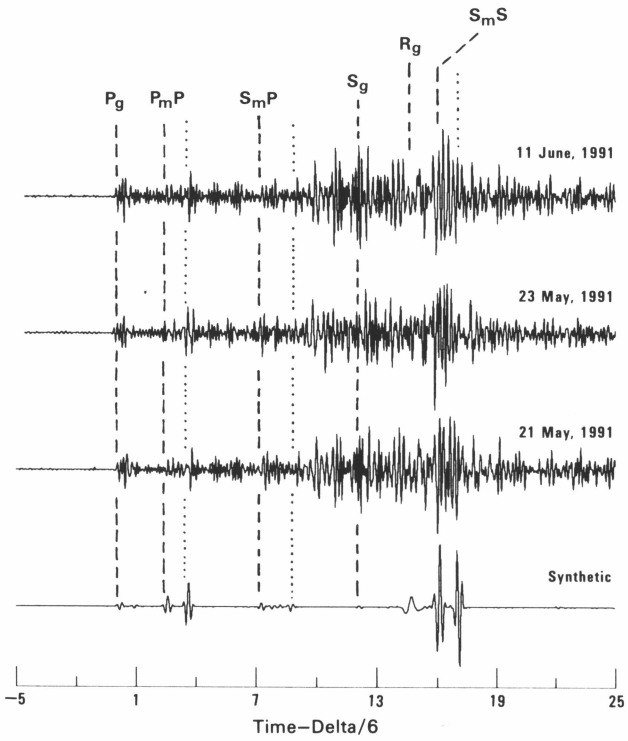


**Figure 3. Observed COO seismograms (top traces) of three earthquakes that took place northwest of Kempsey in May/June 1991, and synthetic (bottom trace) calculated for the model in Table 1 and 3 km focal depth, modified with the crust–mantle boundary at 31 km depth.**

wavetrain. This is confirmed by the bandpass filtered records shown in Figure 4. Based on the comparison of observed with synthetic seismograms several conclusions can be drawn.

The epicentral distance from COO was about 100 km. This follows mainly from the arrival times of *P* and *Rg*. The crustal thickness in the model used to calculate the synthetics was slightly reduced to 31 km. This provides a good fit to the arrival times of Moho reflections (Figs 3, 4). The time differences between Moho reflections and their associated depth phases suggest that focal depth was about 3 km for these events. An attempt was made to put constraints on the focal mechanism of the events using amplitudes of various phases. Note that the phase interpreted as $P_MP$ has quite a small amplitude relative to $sP_MP$. Synthetic seismogram modelling suggests that this is indicative of dip slip faulting along an inclined fault plane. The amplitudes of $S_MS$ and $sS_MS$, on the other hand, are

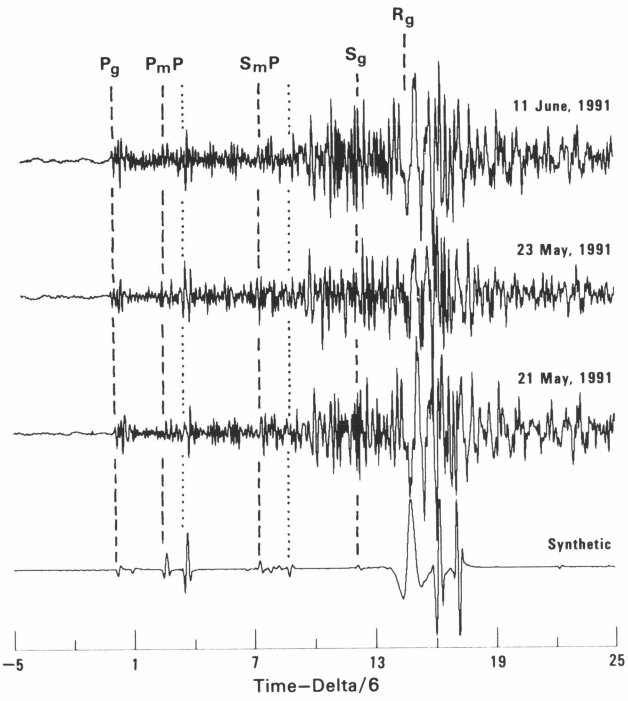


**Figure 4. Bandpass filtered (2.5–11 Hz) records of the seismograms in Figure 3.**

approximately equal (Fig. 4). I searched the full range of dip and strike angles of fault planes to find those that are consistent with the observed amplitudes of $P_MP$, $sP_MP$, $S_MS$, $sS_MS$, and $P_g$. Pure dip slip motion was assumed, and an epicentre-to-station azimuth of 300. The best fitting fault plane strikes N20°E and dips 34° to the east, with the conjugate plane striking 200° and dipping 56° to the west. The synthetic traces in Figures 3 and 4 were obtained for this fault orientation.

## The September 1991 St George (Queensland) earthquakes

Two earthquakes took place northeast of St George (Queensland) in September 1991, the first one ($M_L$ = 4.3) on Sept. 24, 0436 UTC, and the second one ($M_L$ = 4.0) on Sept. 28, 1505 UTC. ASC located the events at 27.52°S, 149.14°E and 27.72°S, 148.98°E, respectively. Focal depths were given as 10 km for the first, and 5 km for the second event. The ARMA digital records of the events are shown in Figure 5. The epicentral distance was about 400 km. The phases $P_n$, $P_g$, and $S_n$ are marked in Figure 5; they correlate well with the synthetic. Figure 6 shows the $P_n$ and $P_g$ phases at an expanded timescale. It is obvious that $P_n$ is followed about 0.6 s later by a larger-amplitude phase. If the first phase is $P_n$ and the second one $sP_n$ then a focal depth of about 2 km is indicated for both events, which significantly differs from the ASC values.

The synthetic seismogram (Figs 5, 6) does not contain the high-frequency components that are present in the observed seismograms. The reflectivity method becomes computationally prohibitive for high frequencies. The point to be made here is the fact that $sP_n$ is observable.

The epicentral area of the St George earthquakes lies in the

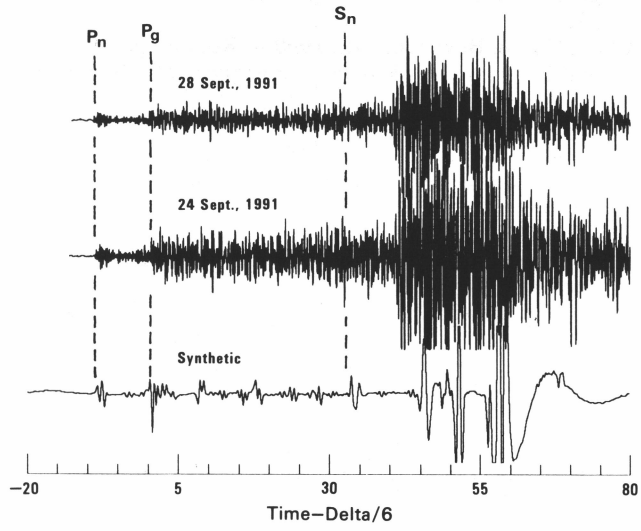


**Figure 5. Observed ARMA seismograms (top traces) of the St George earthquakes that occurred in September 1991 and synthetic (bottom trace) calculated for 2 km focal depth.**

Surat Basin near Riverslea. Sediment thicknesses there are about 1.5 km (Petroleum Resources Assessment and Development Subprogram, 1990). This suggests that the St George earthquakes took place near the top of the basement underlying the basin sediments. I investigated the question of whether the presumed phase $sP_n$ could be in fact a reflection from the sediment-basement interface rather than from the surface. This however is unlikely because reasonable reflection coefficients of the sediment-basement interface are too small to produce the large-amplitude arrivals observed.

The $P_g$ wavetrain, by comparison, is relatively complex in both observed and synthetic seismograms. It would be quite difficult to identify reliably depth phases in the $P_g$ coda. The same applies to the $Lg$ wavetrain. The presence of significant scattered energy following the $P_g$ and $Lg$ arrivals makes it impossible to identify any reflections from the Moho and associated depth phases. It is therefore concluded that, if only vertical-component records from a single station are available, the phase $sP_n$ is probably the only useful body wave phase which allows us to put constraints on focal depth from recordings at several hundred kilometres distance.

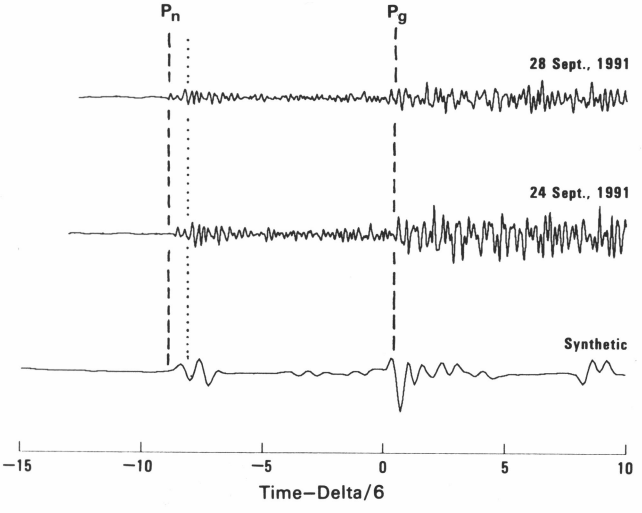


**Figure 6. The $P_n$ and $P_g$ wavetrains of Figure 5 in close up view.**

## Discussion and summary

Synthetic seismograms presented in this paper suggest that a number of depth phases can be observed from local earthquakes at distances up to several hundred kilometres. At epicentral distances of about 100 km or less, reflections from the crust–mantle boundary and associated surface reflections may show up in the seismograms. To be observed over a wide distance range, the crust–mantle transition must be sharp compared with the wavelength of the signals. If the transition is smooth, observable reflections may be restricted to distances near critical. The depth phases are mainly of the type $sX$, where $X$ represents the Moho reflections $P_MP$, $S_MP$, or $S_MS$. Depth phases of the type $pX$ are negligible in amplitude because the $P$–$P$ reflection coefficient of the free surface is much smaller than the $S$–$P$ coefficient. Differential times $sX$–$X$ are shown plotted against focal depth (Fig. 7) for the crustal model in Table 1.

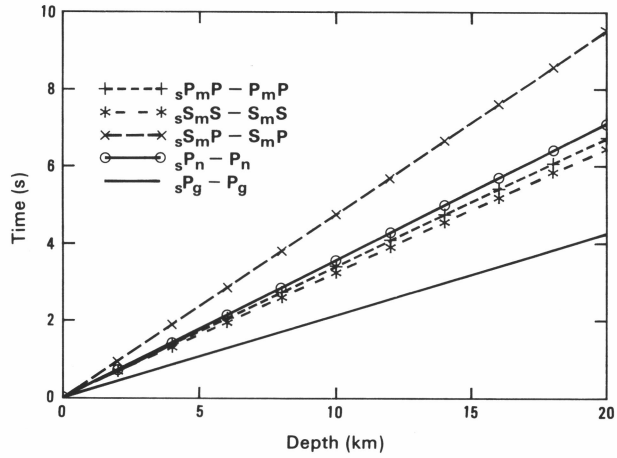


**Figure 7. Differential times $sX - X$ for the phases marked in the legend box against focal depth.**

Synthetic seismograms suggest that another observable depth phase may be $sP_g$ This phase is less sensitive to focal depth than $sX$ as the differential time $sP_g - P_g$ reaches only about half the values of the $sX - X$ times associated with Moho reflections (Fig. 7).

At epicentral distances where $P_n$ is the first arrival, the most useful depth phase is $sP_n$. To be observed at single stations, the time difference $P_g - P_n$ must be large enough so that $sP_n$ arrives well before $P_g$ This means that the epicentral distance must be well beyond the distance at which $P_g$ is overtaken by $P_n$. The differential $sP_n - P_n$ times are also shown in Figure 7.

The method of synthetic seismogram comparison has been applied to earthquakes that occurred in 1991 near Kempsey (New South Wales) and St George (Queensland). Very shallow depths between 2 and 3 km are indicated for these events, while the 1990 Woods Reef earthquake investigated in an earlier study by Bock (in press) was located at a greater depth, near 12 km. A prerequisite for the success of the method described in this paper was the availability

of digital images of the Helicorder chart recordings of the Armidale seismograph. Without this, identification of the various phases contained in the *P* wave coda would have been impossible. The usage of depth-sensitive phases as discussed in this paper and also by Langston (1987) may eventually lead to a much improved picture of the depth distribution of Australian earthquakes

## Acknowledgements

I am grateful to Frank Ludbey who installed the ADC and made it work, to Russell Cuthbertson who drew my attention to the Petroleum Resources Assessment paper, and to Riki Davidson who critically read the manuscript. Marion Leiba from the Australian Seismological Centre is thanked for providing the epicentral location of the May 21 1991 Kempsey earthquake. This research was supported by an Internal Research Grant from the Department of Geology and Geophysics of the University of New England.

## References

Aki, K. & Richards, P.G., 1980 — Quantitative seismology theory and methods. Vol. 1. *Freeman and Co., San Francisco.*

Barbano, M.S., Kind, R. & Zonno, G., 1985 — Focal parameters of some Friuli earthquakes (1976–1979) using complete theoretical seismograms. *Journal of Geophysics* 58, 175–182.

Bock, G., in press — The Woods Reef (New South Wales) earthquake of 14 November 1990: focal mechanism derived from amplitude ratios and synthetic seismograms. *Australian Journal of Earth Sciences.*

Boggs, D., 1991 — A computer based earthquake record acquisition system. *Department of Geology and Geophysics, University of New England, unpublished project report.*

Bowman, J.R., Gibson, G. & Jones, T., 1990 — Aftershocks of the January 22, 1988 Tennant Creek, Australia intraplate earthquakes: evidence for a complex fault geometry. *Geophysical Journal International* 100, 87–97.

Choy, G.L. & Bowman, J.R., 1990 — Rupture process of a multiple main shock sequence: analysis of teleseismic, local, and field observations of the Tennant Creek, Australia, earthquakes of January 22, 1988. *Journal of Geophysical Research* 95, 6867–6882.

Finlayson, D.M. & Collins, C.D.N., in press — Lithospheric velocity structures under New England, northeastern New South Wales — contrasts with other areas of the Tasman Orogen. *Australian Journal of Earth Sciences.*

Fredrich, J., McCaffrey, R. & Denham, D., 1988 — Source parameters of seven large Australian earthquakes determined by body waveform inversion. *Geophysical Journal* 95, 1–13.

Kind, R., 1978 — The reflectivity method for a buried source. *Journal of Geophysics* 44, 603–612.

Kind, R., 1979a — Observations of sPn from Swabian Alb earthquakes at the GRF array. *Journal of Geophysics* 45, 337–340.

Kind, R., 1979b — Extensions of the reflectivity method. *Journal of Geophysics* 45, 373–380.

Langston, C.A., 1987 — Depth of faulting during the 1968 Meckering, Australia, earthquake sequence determined from waveform analysis of local seismograms. *Journal of Geophysical Research* 92, 11561–11574.

McEvilly, T.V. & Majer, E.L., 1982 — ASP: an automated seismic processor for microearthquake networks. *Bulletin of the Seismological Society of America* 72, 303–325.

Petroleum Resources Assessment and Development Subprogram, 1990 — Petroleum Resources of Queensland (Review to June 30, 1989). *Queensland Department of Resource Industry Review Series, Department of Resource Industries, Queensland.*

Zonno, G. & Kind, R., 1984 — Depth determination of North Italian earthquakes using Gräfenberg data. *Bulletin of the Seismological Society of America* 74, 1645–1659.